NewsStand, Inc. - Today's Way To Read Publications--Digitally - Microsoft Internet Explorer

LETTERS

Strong quantum-confined Stark effect in germanium quantum-well structures on silicon

Yu-Hsuan Kuo[1], Yong Kyu Lee[1], Yangsi Ge[1], Shen Ren[1], Jonathan E. Roth[1], Theodore I. Kamins[1,2], David A. B. Miller[1] & James S. Harris[1]

Silicon is the dominant semiconductor for electronics, but there is now a growing need to integrate such components with optoelectronics for telecommunications and computer interconnections[1]. Silicon-based optical modulators have recently been successfully demonstrated[2,3]; but because the light modulation mechanisms in silicon[4] are relatively weak, long (for example, several millimetres) devices[2] or sophisticated high-quality-factor resonators[3] have been necessary. Thin quantum-well structures made from III-V semiconductors such as GaAs, InP and their alloys exhibit the much stronger quantum-confined Stark effect (QCSE) mechanism[5], which allows modulator structures with only micrometres of optical path length[6,7]. Such III-V materials are unfortunately difficult to integrate with silicon electronic devices. Germanium is routinely integrated with silicon in electronics[8], but previous silicon–germanium structures have also not shown strong modulation effects[9–13]. Here we report the discovery of the QCSE, at room temperature, in thin germanium quantum-well structures grown on silicon. The QCSE here has strengths comparable to that in III-V materials. Its clarity and strength are particularly surprising because germanium is an indirect gap semiconductor; such semiconductors often display much weaker optical effects than direct gap materials (such as the III-V materials typically used for optoelectronics). This discovery is very promising for small, high-speed[14], low-power[15–17] optical output devices fully compatible with silicon electronics manufacture.

Quantum wells are thin (for example, 10 nm) layers of semiconductors surrounded by barrier materials. Usually the barriers are chosen to confine electrons in the conduction band and holes (or absences of electrons) in the valence band inside the quantum well; this is called type-I band alignment. The QCSE gives strong spectral shifts of the optical absorption edge with applied electric field near the direct bandgap (that is, a band structure in which the energy minima for electrons and holes lie at the same momentum) in such type-I quantum wells[18]. Usually these relevant band minima are at zero momentum (the Γ point, or 'zone centre').

The QCSE is routinely used in high-performance quantum-well modulators for telecommunications. It possesses a number of attractive properties that allow for modulators with only micrometres of path length that can be incorporated into large arrays (for example, >38,000 devices) attached to complementary metal-oxide-semiconductor (CMOS) silicon circuits[6], as well as devices at telecommunications wavelengths of ~1.5 μm (ref. 7). Waveguide QCSE devices typically have lengths of only ~100–400 μm (see, for example, ref. 14). Recent work[19] has demonstrated devices in InGaAs/InP quantum wells without waveguides that exhibit useful modulation at telecommunications wavelengths for <1 V drive, and with the relaxed alignment required for practical packaging. QCSE devices do not require carrier injection, and are typically operated as reverse-biased diodes. The resulting low power dissipation—of the order of 10 mW per channel—allows large arrays of optical interconnects operating at high data rates from silicon chips[15–17]. Theoretically, the QCSE is thought to operate at subpicosecond times[20,21], and devices with >50 GHz modulation bandwidth have been demonstrated[14].

Unlike the III-V compounds typically used for QCSE modulators, both silicon and germanium have indirect lowest-energy bandgaps (meaning that the electron and hole energy minima have different momenta). Previously, type-I SiGe/Si quantum wells have shown no or inefficient QCSE[9–11], whereas SiGe/Si quantum wells[12] and Ge/Si quantum dots[13] (both of which have type-II band alignment in which the electrons and holes have minimum energy in different material layers) can exhibit large shifts of optical transitions with electric field, but have low absorption efficiency. Here we demonstrate clear quantum confinement effects in the optical absorption spectra of Ge quantum wells, associated with zone centre transitions, and in addition a clear and strong QCSE electroabsorption. Though germanium's lowest bandgap is indirect, we exploit its direct bandgap at ~0.8 eV at room temperature; the band structure associated with this direct bandgap is qualitatively identical to that in III-V QCSE materials. There is also indirect absorption present at the same and lower photon energies, but it is much weaker, allowing the direct optical absorption to dominate.

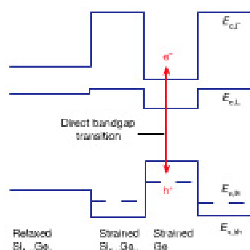

Figure 1 | The bandgap structure of a Ge/SiGe quantum well (not to scale). $E_{c,\Gamma}$ and $E_{c,L}$ are the energies of the bottom of the conduction band at zone centre (Γ point) and at the L valleys, respectively. $E_{v,lh}$ and $E_{v,hh}$ are the energies of the tops of the light-hole and heavy-hole valence bands, respectively. The Ge/$Si_{0.15}Ge_{0.85}$ quantum well on relaxed $Si_{0.1}Ge_{0.9}$ has type-I alignment at the zone centre and quantum-confines carriers inside the Ge well.

[1]Solid State and Photonics Laboratory, Department of Electrical Engineering, Stanford University, Stanford, California 94305, USA. [2]Quantum Science Research, Hewlett-Packard Laboratories, Palo Alto, California 94304, USA.

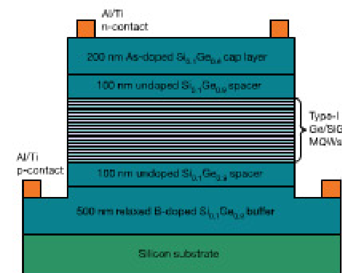

Figure 2 | Schematic diagram of a p-i-n diode. The cross-sectional view shows the structure of strained Ge/SiGe multiple quantum wells (MQWs) grown on silicon on relaxed SiGe direct buffers (not to scale). In the measurements, light from a monochromator is incident on the top surface (that is, in a 'surface-normal' configuration) on the open area inside the rectangular frame top electrode (that is, between the portions of the Al/Ti n-contacts shown in this cross-section).

We use strain-balanced Ge/SiGe multiple quantum wells (MQWs) grown on a relaxed Ge-rich SiGe buffer on silicon, giving type-I alignment at the Γ point. In strain-balanced structures, the average silicon concentration in the Ge/SiGe MQW layers equals that of the buffer layer, allowing the growth of thick structures. Figure 1 shows the resulting bandgap alignment. The band discontinuities of the heavy hole, light hole, and electron at the Γ point between our wells and barriers are calculated to be 101 meV, 47 meV, and 400 meV respectively, based on refs 22–24 with linear interpolation of the direct bandgap of SiGe between Si (to the Γ-2′ band) and Ge. Note that this 400 meV Γ-point band discontinuity provides strong electron quantum confinement in the conduction band. There are, of course, lower-energy conduction band minima (L valleys) in the SiGe barriers. For quantum confinement, however, we expect the relevant bands in the barriers to be those with similar unit cell symmetries, as we expect that it is only to such bands that strong tunnelling can exist. Hence, we consider here the bands at the Γ point in the barriers for the calculation of quantum confinement effects. Because the Γ point in Ge wells is higher than the L valleys in the SiGe barriers, we do however expect that, even though the Γ point electron quantum well is relatively deep, electrons generated in the Ge wells will be rapidly scattered out into those L valleys where they can be swept out by electric fields (though not so fast as to prevent the quantum confinement exploited in optical absorption).

Figure 2 shows the Ge/SiGe MQW p-i-n diode structure. The layers are grown sequentially in a commercially available, single-wafer, cold-wall, reduced-pressure, chemical vapour deposition (RPCVD) reactor, using hydrogen carrier gas and silane and germane precursor gases. We use four-inch, boron-doped, (001)-oriented silicon wafer substrates with resistivity 10–20 Ω cm. After an *in situ* high-temperature cleaning, the layers are grown at 400 °C, with annealing at higher temperatures. Two 250-nm $Si_{0.1}Ge_{0.9}$ films doped with 5×10^{18} cm^{-3} boron atoms are grown sequentially and annealed at 850 °C for 30 min and 700 °C for 5 min, respectively, to reduce dislocations caused by the lattice mismatch and to form relaxed p-type buffer layers. A 100 nm undoped $Si_{0.1}Ge_{0.9}$ spacer layer is grown, followed by ten pairs of MQWs (10 nm Ge well/16 nm $Si_{0.15}Ge_{0.85}$ barrier) and another 100 nm undoped $Si_{0.1}Ge_{0.9}$ spacer layer. Finally, the structure is capped by an arsenic-doped $Si_{0.1}Ge_{0.9}$ layer with a doping level of 10^{19} cm^{-3}. Each wafer is then patterned by standard lithography and dry-etched to form square mesa structures with widths ranging from 200 to 1,400 μm. Al/Ti metal is evaporated, lifted off, and rapid-thermal-annealed to form rectangular frame ohmic contacts. Because the top As-doped (n-type) SiGe layer is expected to be strongly conducting, the electric field should be essentially perpendicular to the quantum wells throughout the structure. All materials, processing equipment and temperatures used are compatible with the processes used in fabricating CMOS silicon electronics.

We measure photocurrent spectra at room temperature for different diode reverse bias voltages using a chopped quartz-tungsten-halogen light bulb source with a 0.25 m monochromator with a 600 lines mm^{-1} grating and a 400 μm slit, and a lock-in amplifier. The light is incident normal to the surface, with random polarization in the surface plane. As in other quantum-well structures, we expect light- and heavy-hole transitions both to be allowed in this configuration. The responsivity (current per unit optical power) inside the device is deduced from the light intensity incident upon the open area of the mesa surface, correcting for surface reflection. The corresponding effective absorption coefficient spectra (Fig. 3) are calculated assuming one electron of current for every absorbed photon, as is common in fully depleted p-i-n diodes. (Presuming that there is no avalanche gain, this assumption at worst underestimates the absorption. The independence of the photocurrent on bias at high photon energies (for example, 0.94 eV) suggests no bias dependence of the number of electrons per photon, and hence no avalanching.) Clear quantum confinement is seen, with strong exciton peaks that we assign to electron-to-heavy-hole (e–hh; ~0.88 eV at 0 V) and electron-to-light-hole (e–lh; ~0.91 eV at 0 V) transitions. The effective absorption coefficient at the e–hh exciton peak, calculated on the basis of the total thickness of the wells and the barriers (~0.26 μm), is 6,320 cm^{-1}. The half-width at half-maximum of the heavy-hole exciton peak is only ~8 meV, and the heavy-hole exciton peak is still clearly resolved even at 8×10^4 V cm^{-1} (3 V bias), indicating that the electric field is uniform inside the structure, which in turn implies very low background doping in the intrinsic region. The absorption edge at zero bias is ~80 meV higher than that of bulk unstrained Ge; this shift is near the calculated sum from quantum-well confinement (56 meV) and strain-induced shifts (36 meV)[23]. As the quantum confinement energy originates primarily from the electron, the clarity of this quantum shift shows that the (quantum-mechanical) confinement at the Γ point is strong,

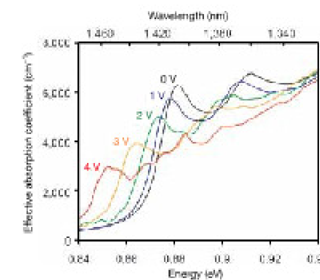

Figure 3 | Effective absorption coefficient spectra. Strong QCSE is observed at room temperature with reverse bias from zero to 4 V. The thickness for effective absorption coefficient calculations is based on the combination of Ge well and SiGe barrier thicknesses.

NATURE 10/27/2005 Section: Letters to Nature Page: 1334/1335
Интернет
пуск The Bat! NewsStand, I... NewsStand, I... Adobe Acrob... EN 11:06

NewsStand, Inc. - Today's Way To Read Publications--Digitally - Microsoft Internet Explorer

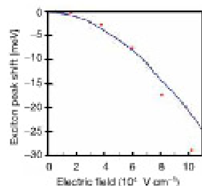

Figure 4 | Shifts of exciton peaks. Comparison of heavy-hole exciton peak shift from measurements (filled squares) and tunnelling resonance calculations (sum of electron and hole level shifts) (line).

despite the possibility of scattering to the lower indirect valleys.

With a reverse bias from 0 to 4 V, both peaks are red shifted by the QCSE. The e–hh exciton is shifted from 1,408 nm (0 V) to 1,456 nm (4 V). The maximum effective absorption coefficient change is 2,800 cm^{-1} at 1,438 nm under 3 V bias. This is, to our knowledge, the first efficient electro-absorption modulation observed in group-IV materials, and its performance is comparable to high-quality (direct gap) III-V materials at similar wavelengths (see, for example, ref. 19). The clarity of the exciton peaks in the presence of a field is actually better than that of typical III-V structures at such wavelengths[19], and the electroabsorption shows much clearer shifts than previous electroabsorption measurements in indirect III-V materials[25]. With a 4 V bias, the absorption coefficient contrast is greater than 3 over a bandwidth ranging from 1,443 to 1,471 nm, with a peak value of 4.69 at 1,461 nm.

The possibility of operating different quantum-well designs at, say, 1,550 nm, which is compatible with long-distance telecommunications, will be the subject of future work. We also anticipate that waveguide modulator structures will be realizable using appropriate materials for waveguide cladding layers.

The measured shift agrees with simulated results (Fig. 4) obtained via the tunnelling resonance method[5,18]. In addition, we evaluated the exciton binding energy shift as in ref. 18, using numerically evaluated electron and hole wavefunctions, though this correction is <1 meV and is neglected here. We used a Γ-valley electron effective mass of $0.041m_0 + 0.115(1-x)m_0$, and a heavy-hole effective mass of $0.28m_0 + 0.21(1-x)m_0$, where m_0 is the free electron mass and x is the Ge concentration[26,27] (the relevant silicon (001) hole mass is based on Luttinger parameters[28]).

We have demonstrated efficient QCSE in silicon-based structures, using strained Ge MQWs. The behaviour of the exciton peaks, the band edge shift and the shift in absorption coefficient are comparable to those observed in III-V materials at similar wavelengths. Our materials and fabrication processes are completely CMOS compatible and suitable for mass production. This approach is therefore very promising for silicon-based electro-absorption modulators operating at high speed, low power, low operating voltage and with small device areas.

Received 8 July; accepted 5 September 2005.

1. Miller, D. A. B. Rationale and challenges for optical interconnects to electronic chips. *Proc. IEEE* **88**, 728–749 (2000).
2. Liu, A. *et al.* A high-speed silicon optical modulator based on a metal-oxide-semiconductor capacitor. *Nature* **427**, 615–618 (2004).
3. Xu, Q., Schmidt, B., Pradhan, S. & Lipson, M. Micrometre-scale silicon electro-optic modulator. *Nature* **435**, 325–327 (2005).
4. Soref, R. A. & Bennett, B. R. Electrooptical effects in silicon. *IEEE J. Quant. Electron.* **23**, 123–129 (1987).
5. Miller, D. A. B. *et al.* Band-edge electroabsorption in quantum well structures: the quantum-confined Stark effect. *Phys. Rev. Lett.* **53**, 2173–2176 (1984).
6. Arad, U. *et al.* Development of a large high-performance 2-D array of GaAs-AlGaAs multiple quantum-well modulators. *IEEE Photon. Tech. Lett.* **15**, 1531–1533 (2003).
7. Liu, C. P. *et al.* Design, fabrication and characterisation of normal-incidence 1.56-μm multiple-quantum-well asymmetric Fabry-Perot modulators for passive picocells. *IEICE Trans. Electron. E* **86C**, 1281–1289 (2003).
8. Cressler, J. D. SiGe HBT technology: a new contender for Si-Based RF and microwave circuit applications. *IEEE Trans. Microwave Theory Tech.* **46**, 572–589 (1998).
9. Qasaimeh, O., Bhattacharya, P. & Croke, E. T. SiGe-Si quantum-well electroabsorption modulators. *IEEE Photon. Tech. Lett.* **10**, 807–809 (1998).
10. Miyake, Y., Kim, J. Y., Shiraki, Y. & Fukatsu, S. Absence of Stark shift in strained $Si_{1-x}Ge_x$/Si type-I quantum wells. *Appl. Phys. Lett.* **68**, 2097–2099 (1996).
11. Li, C. *et al.* Observation of quantum-confined Stark shifts in SiGe/Si type-I multiple quantum wells. *J. Appl. Phys.* **87**, 8195–8197 (2000).
12. Park, J. S., Karunasiri, R. P. G. & Wang, K. L. Observation of large Stark shift in Ge_xSi_{1-x}/Si multiple quantum wells. *J. Vac. Sci. Technol. B* **8**, 217–220 (1990).
13. Yakimov, A. I. *et al.* Stark effect in type-II Ge/Si quantum dots. *Phys. Rev. B* **67**, 125318 (2003).
14. Lewen, R., Irmscher, S., Westergren, U., Thylen, L. & Eriksson, U. Segmented transmission-line electroabsorption modulators. *J. Lightwave Technol.* **22**, 172–179 (2004).
15. Krishnamoorthy, A. V. & Miller, D. A. B. Scaling optoelectronic-VLSI circuits into the 21st century: a technology roadmap. *IEEE J. Select. Top. Quant. Electron.* **2**, 55–76 (1996).
16. Kibar, O., Van Blerkom, D. A., Fan, C. & Esener, S. C. Power minimization and technology comparisons for digital free-space optoelectronic interconnections. *J. Lightwave Technol.* **17**, 546–555 (1999).
17. Cho, H., Kapur, P. & Saraswat, K. C. Power comparison between high-speed electrical and optical interconnects for interchip communication. *J. Lightwave Technol.* **22**, 2021–2033 (2004).
18. Miller, D. A. B. *et al.* Electric field dependence of optical absorption near the bandgap of quantum well structures. *Phys. Rev. B* **32**, 1043–1060 (1985).
19. Helman, N. C., Roth, J. E., Bour, D. P., Altug, H. & Miller, D. A. B. Misalignment-tolerant surface-normal low-voltage modulator for optical interconnects. *IEEE J. Select. Top. Quant. Electron.* **11**, 338–342 (2005).
20. Schmitt-Rink, S., Chemla, D. S., Knox, W. H. & Miller, D. A. B. How fast is excitonic electroabsorption? *Opt. Lett.* **15**, 60–62 (1990).
21. Maslov, A. V. & Citrin, D. S. Quantum-well optical modulator at terahertz frequencies. *J. Appl. Phys.* **93**, 10131–10133 (2003).
22. Galdin, S., Dollfus, P., Aubry-Fortuna, V., Hesto, P. & Osten, H. J. Band offset predictions for strained group IV alloys: $Si_{1-x-y}Ge_xC_y$ on Si(001) and $Si_{1-x}Ge_x$ on $Si_{1-z}Ge_z$(001). *Semicond. Sci. Technol.* **15**, 565–572 (2000).
23. Rieger, M. M. & Vogl, P. Electronic-band parameters in strained $Si_{1-x}Ge_x$ alloys on $Si_{1-y}Ge_y$ substrates. *Phys. Rev. B* **48**, 14276–14287 (1993).
24. Schaffler, F. High-mobility Si and Ge structures. *Semicond. Sci. Technol.* **12**, 1515–1549 (1997).
25. Goossen, K. W., Yan, R. H., Cunningham, J. E. & Jan, W. Y. $Al_xGa_{1-x}As$-AlAs quantum well surface-normal electroabsorption modulators operating at visible wavelengths. *Appl. Phys. Lett.* **59**, 1829–1831 (1991).
26. Crow, G. C. & Abram, R. A. Monte Carlo simulations of hole transport in SiGe and Ge quantum wells. *Semicond. Sci. Technol.* **15**, 7–14 (2000).
27. Dresselhaus, G., Kip, A. F. & Kittel, C. Cyclotron resonance of electrons and holes in silicon and germanium crystals. *Phys. Rev.* **98**, 368–384 (1955).
28. Lawaetz, P. Valence-band parameters in cubic semiconductors. *Phys. Rev. B* **4**, 3460–3467 (1971).

Acknowledgements We thank V. Lordi for help with photocurrent setup. We also thank J. Fu, T. Krishnamohan and X. Yu for help with device fabrication and material characterization. Finally, we thank G. S. Solomon and D. S. Gardner for discussions. This work was supported by Intel Corporation and the DARPA/ARO EPIC programme.

Author Information Reprints and permissions information is available at npg.nature.com/reprintsandpermissions. The authors declare no competing financial interests. Correspondence and requests for materials should be addressed to Y.-H.K. (yhkuo@stanford.edu).

LETTERS

Unidirectional molecular motor on a gold surface

Richard A. van Delden[1], Matthijs K. J. ter Wiel[1], Michael M. Pollard[1], Javier Vicario[1], Nagatoshi Koumura[1] & Ben L. Feringa[1]

Molecules capable of mimicking the function of a wide range of mechanical devices have been fabricated, with motors that can induce mechanical movement attracting particular attention[1,2]. Such molecular motors convert light or chemical energy into directional rotary or linear motion[3–10], and are usually prepared and operated in solution. But if they are to be used as nanomachines that can do useful work, it seems essential to construct systems that can function on a surface, like a recently reported linear artificial muscle[11]. Surface-mounted rotors have been realized and limited directionality in their motion predicted[12,13]. Here we demonstrate that a light-driven molecular motor capable of repetitive unidirectional rotation[14] can be mounted on the surface of gold nanoparticles. The motor design[14] uses a chiral helical alkene with an upper half that serves as a propeller and is connected through a carbon–carbon double bond (the rotation axis) to a lower half that serves as a stator. The stator carries two thiol-functionalized 'legs', which then bind the entire motor molecule to a gold surface. NMR spectroscopy reveals that two photo-induced *cis-trans* isomerizations of the central double bond, each followed by a thermal helix inversion to prevent reverse rotation, induce a full and unidirectional 360° rotation of the propeller with respect to the surface-mounted lower half of the system.

Inspired by the ATP-ase system[15], we constructed an artificial surface-mounted motor schematically shown in Fig. 1a. The design of the motor molecule **1** is based on a second-generation[14] light-driven rotary motor **2** with a symmetric lower half bearing two methoxy substituents (Fig. 1b). Replacing these groups by two C_8-spacers terminated with thiols (as shown in structure **1**) allowed self-assembly onto a gold surface, providing **1-Au**. Gold nanoparticles are particularly appropriate for our purpose, as chromophore functionalized nanoparticles are well studied[16] and photochromism of azobenzenes[17] and electrochemical switching of rotaxanes[18] attached to such nanoparticles has been demonstrated. Two points of attachment are essential to prevent uncontrolled thermal rotation of the entire system with respect to the surface. The C_8-spacer should diminish direct (electronic) interaction between the chromophores and the Au surface (which might influence the excited state processes) and give the separate photo-active moieties sufficient free volume to perform the anticipated rotary motion. On the basis of the dynamic processes in structurally related molecular motors[14], **1-Au** was expected to exhibit photochemical and thermal isomerization processes, as shown in Fig. 1c.

Two energetically uphill photochemical isomerization steps (steps 1 and 3 in Fig. 1) each followed by an energetically downhill irreversible thermal helix inversion step (steps 2 and 4 in Fig. 1) result in a full 360° rotation of one half of the molecule with respect to the other. The direction of rotation is controlled by the configuration at the stereogenic centre. Crucial is a strong energetic preference for the methyl substituent to adopt a pseudo-axial orientation. Irradiation

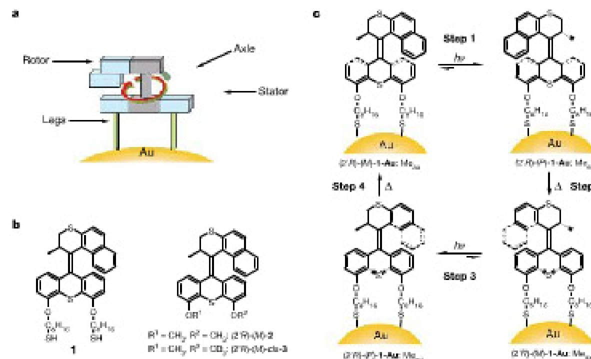

Figure 1 | Molecular motor anchored to a surface. **a**, Design of a surface-bound rotary motor. The system consists of a rotor connected via an axle (axis of rotation) to a stator part that is bound to a gold surface via two legs. **b**, Structure of motor 1 for surface studies and 2, 3 for solution studies; 1-Au denotes motor molecule 1 assembled onto Au. *R* denotes absolute configuration at the stereogenic centre; *M* and *P* denote helicity of the molecule. **c**, The four-state unidirectional rotation of functionalized nanoparticle 1-Au is shown (*hν*, photochemical step; Δ, thermal step). The photoisomerizations were induced by irradiation at λ ≥ 280 nm or λ = 365 nm. Me_{ax} indicates the pseudo-axial orientation of the methyl substituent, Me_{eq} indicates the unstable pseudo-equatorial orientation of the methyl substituent.

[1]Department of Organic Chemistry, Stratingh Institute, University of Groningen, Nijenborgh 4, 9747 AG Groningen, The Netherlands.

NATURE 10/27/2005 Section: Letters to Nature Page: 1336/1337
Интернет
пуск The Bat! NewsStand, I... NewsStand, I... 2710 5.pdf EN 11:07